In vivo imaging of glucose uptake and metabolism in tumors

SUPPLEMENTAL INFORMATION

Simon Walker-Samuel[1], Rajiv Ramasawmy[1], Francisco Torrealdea[1,2], Marilena Rega[2], Vineeth Rajkumar[3], S. Peter Johnson[3], Simon Richardson[1], Miguel Gonçalves[1], Harold G. Parkes[4], Erik Årstad[5], David L. Thomas[2], R. Barbara Pedley[3], Mark F. Lythgoe[1]*, Xavier Golay[2]*

[1]UCL Centre for Advanced Biomedical Imaging, Division of Medicine and Institute of Child Health, London, UK
[2]UCL Institute of Neurology, London, UK
[3]UCL Cancer Institute, London, UK
[4]Cancer Research UK and EPRSC Cancer Imaging Centre, The Institute of Cancer Research and Royal Marsden NHS Foundation Trust, Sutton, Surrey, UK
[5]UCL Department of Chemistry, London, UK
** MFL and XG jointly directed this research*

SUPPLEMENTAL FIGURES

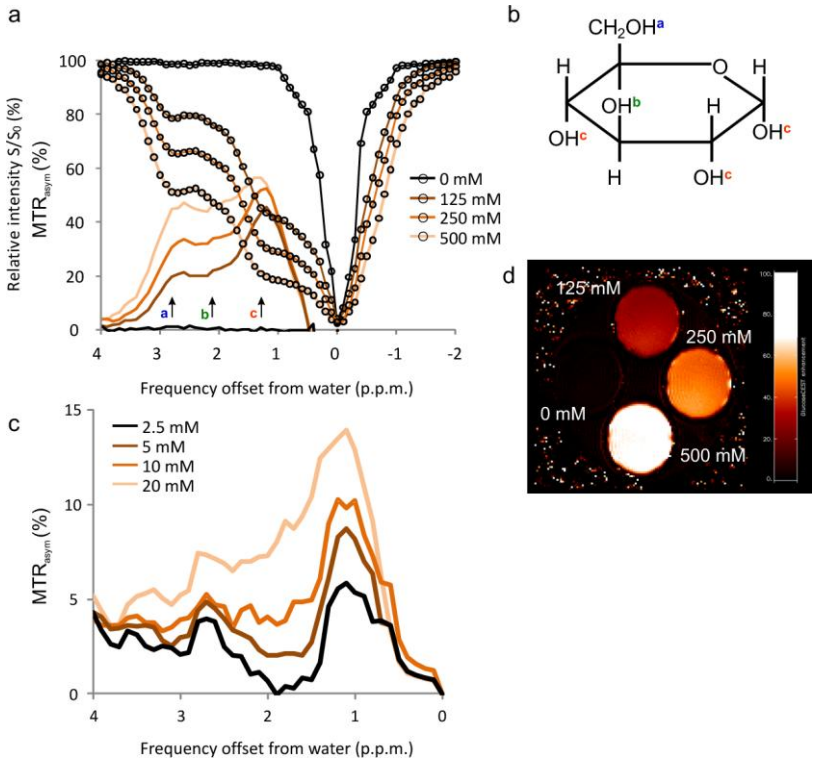

Supplemental Figure 1. *In vitro* measurements of glucose z- and MTR_{asym} spectra. a) z-spectra from four glucose solutions (circular markers, pH = 7.2, 37°C), with MTR_{asym} spectra overlaid (solid lines, no markers), acquired at 9.4 T. Peaks corresponding to exchangeable protons can be observed in MTR_{asym} spectra at approximately 1.2, 2.1 and 2.9 p.p.m., which is in agreement with those found by van Zijl *et al*. b) Schematic diagram of a glucose molecule showing the location of hydroxyl groups containing labile protons. c) MTR_{asym} spectra from low glucose concentrations (2.5, 5, 10 and 20 mM), which show clear CEST effects, even at the lowest concentration. d) An image showing the glucoCEST effect in four glucose solutions (pH = 7.2, 37°C). These were produced by integration of MTR_{asym} spectra between 0.75 and 4 p.p.m. for each pixel, and show a clear increase in the CEST effect for increasing glucose concentration.

Nature Medicine: doi:10.1038/nm.3252

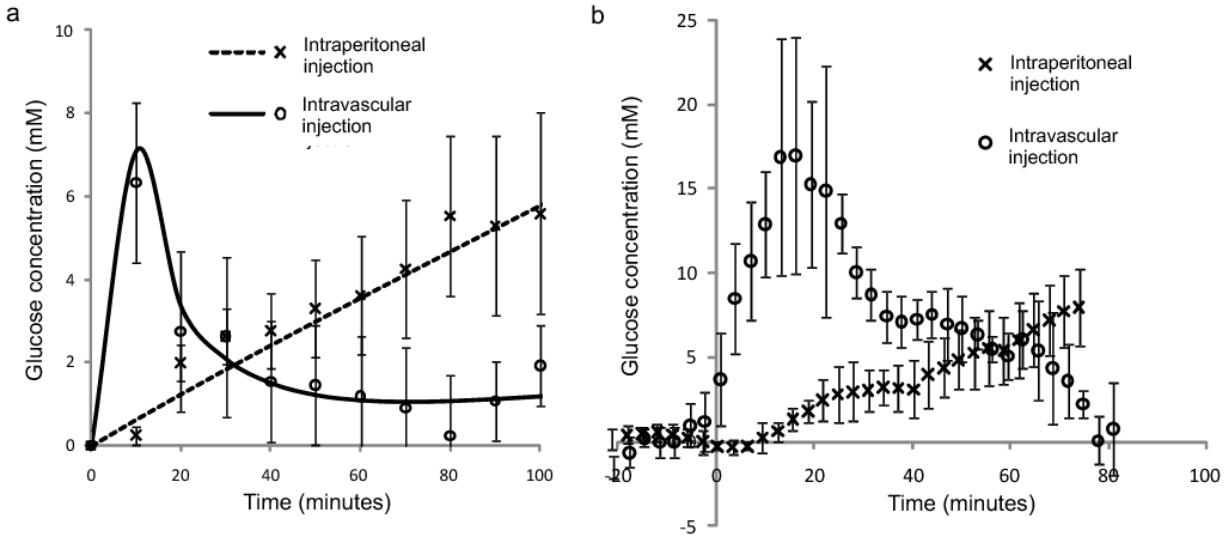

Supplemental Figure 2. Comparison of a) the change in whole-tumor glucoCEST enhancement (GCE, acquired using the EXPRESS sequence and fitted to Equ. 2), and b) direct sampling from a tail vein using a hand-held blood glucose monitor. Averaged data are shown from both intravenous injection (i.v., *n* = 5) and intraperitoneal injection (i.p., *n* = 5) in mice bearing SW1222 human colorectal tumors. Clear differences can be observed in glucose uptake between the two routes of administration, as would be expected, and a close correspondence can be seen between glucoCEST enhancement profiles and blood glucose measurements. Error bars represent the standard error in each measurement. Due to the slower glucose kinetics observed with i.p. administration, which are advantageous for the temporal resolution of glucoCEST acquisitions (~15 minutes), i.p. glucose administration was chosen for all further experiments.

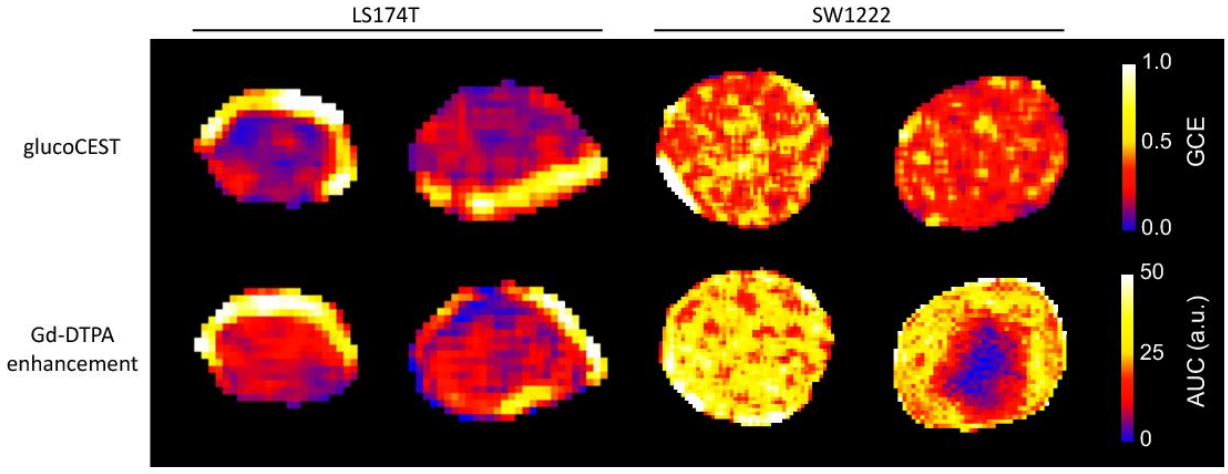

Supplemental Figure 3. Images of glucoCEST and Gd-DTPA uptake in two human colorectal tumor xenograft models (LS174T and SW1222), at 60 minutes following i.p. injection. Whilst some similarities can be observed, marked differences are also evident in enhancement patterns between Gd-DTPA, a commonly used MRI contrast agent, and glucose.

Nature Medicine: doi:10.1038/nm.3252

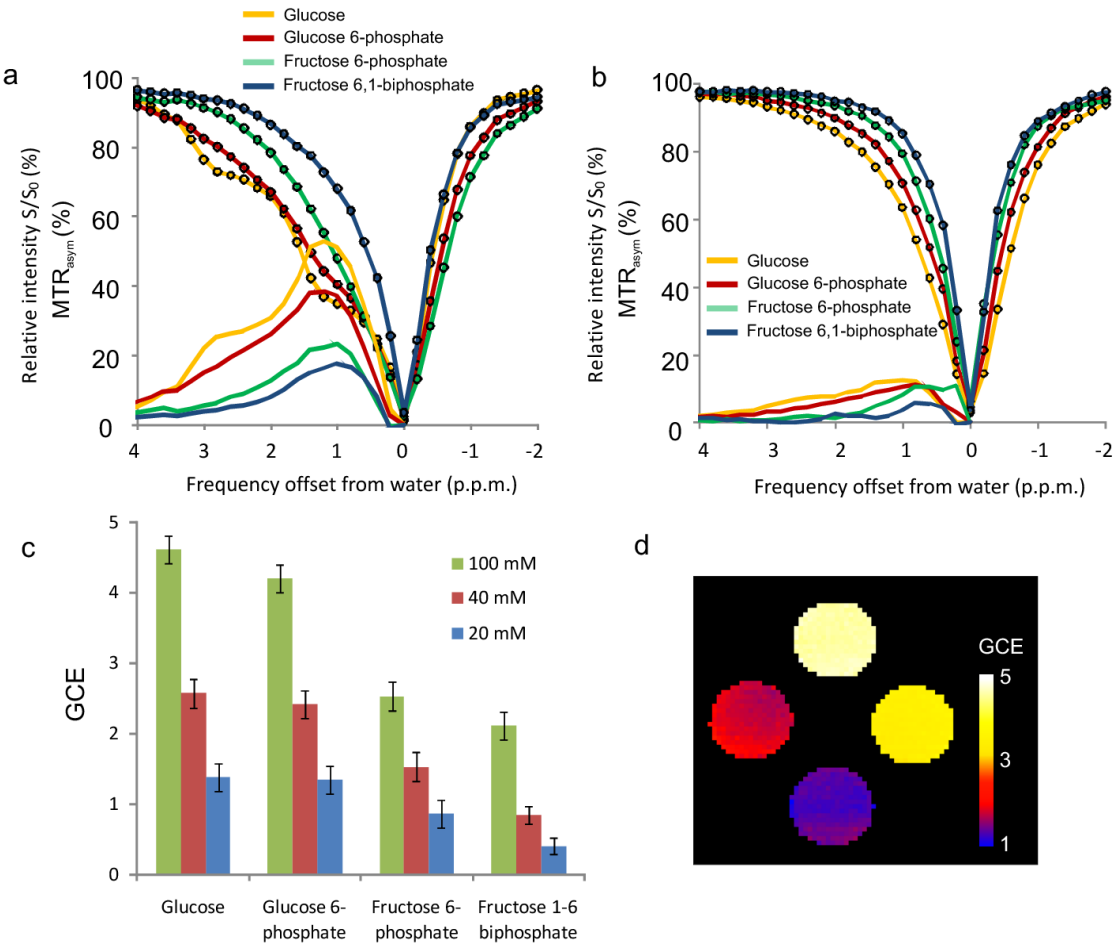

Supplemental Figure 4. Z- and MTR_{asym} spectra from glucose, glucose 6-phosphate, fructose 6-phosphate and fructose 6,1-biphosphate, at concentrations of 100 mM (a) and 40 mM (b). The magnitude of measured GCE for each of these molecules is shown in (c), which indicates that glucose and glucose-6-phosphate have similar GCE, and fructose 6-phosphate and fructose 6,1-biphosphate have a smaller GCE. The number of hydroxyl groups in these molecules is 5 (glucose), 4, (glucose 6-phosphate), 4 (fructose 6-phosphate) and 3 (fructose 6,1-biphosphate), yet the measured GCE, relative to glucose, was 1, 0.94 ± 0.02, 0.59 ± 0.02 and 0.36 ± 0.05, respectively, suggesting that CEST exchange effect is modified in each molecule. A GCE image for a phantom containing each molecule (100 mM, pH = 7.4 and 37 °C) is shown in (d).

Nature Medicine: doi:10.1038/nm.3252

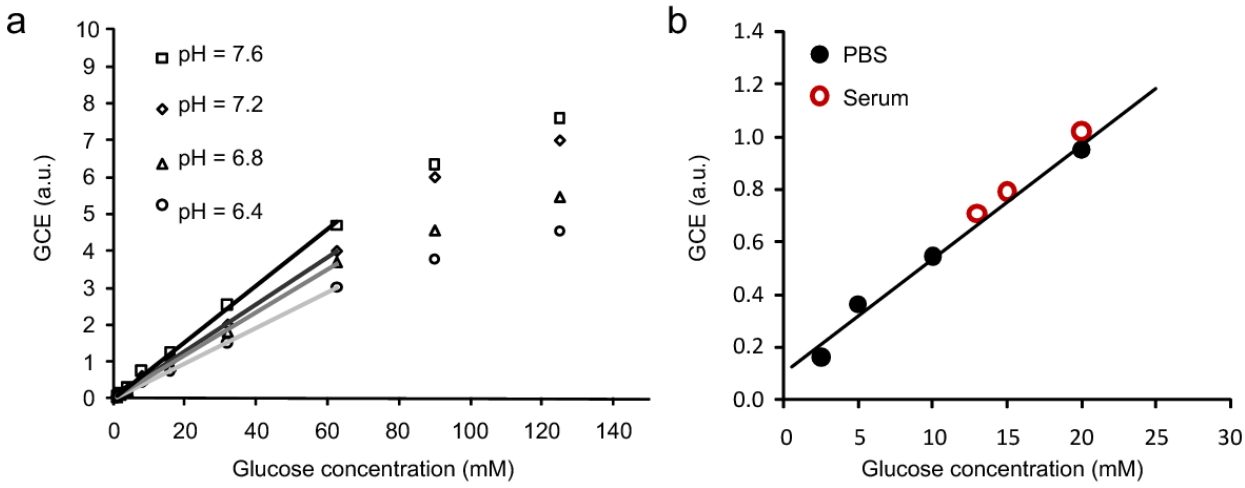

Supplemental Figure 5. GlucoCEST enhancement as a function of glucose concentration, measured *in vitro*. a) The increase in GCE for four different pH values, each fitted using linear regression. By spatially averaging the GCE signal in each phantom, a precise, linear relationship between glucose concentration and GCE can be seen in the phantom data up to a concentration of between 60 and 100 mM. Above this concentration, the rate of increase of GCE with glucose concentration decreases due to the onset of complete saturation of water protons . From linear least squares regression of the linear region (1 to 60 mM), the gradients of these data were measured to be 0.52 ± 0.03, 0.58 ± 0.02, 0.63 ± 0.02 and 0.75 ± 0.03 mM^{-1} (pH = 6.4, 6.8, 7.2 and 7.6, respectively). It is acknowledged that the linear modeling of these data could be improved upon, for example by fitting a Michaelis-Menten type of kinetic model, such as described by Ali *et al* [1], which would improve the characterization of phantoms with glucose concentrations greater than 60 mM. The relationship between GCE and glucose concentration was found to be linear for concentrations up to 60 mM, but deviated from linearity at higher concentrations. b) GCE *vs* glucose concentration for lower concentration glucose solutions than shown in (a), in both PBS and blood serum. Both of these data are linear within the measured range of glucose concentration, and the signal from blood serum does not differ significantly from that of water solutions.

Nature Medicine: doi:10.1038/nm.3252

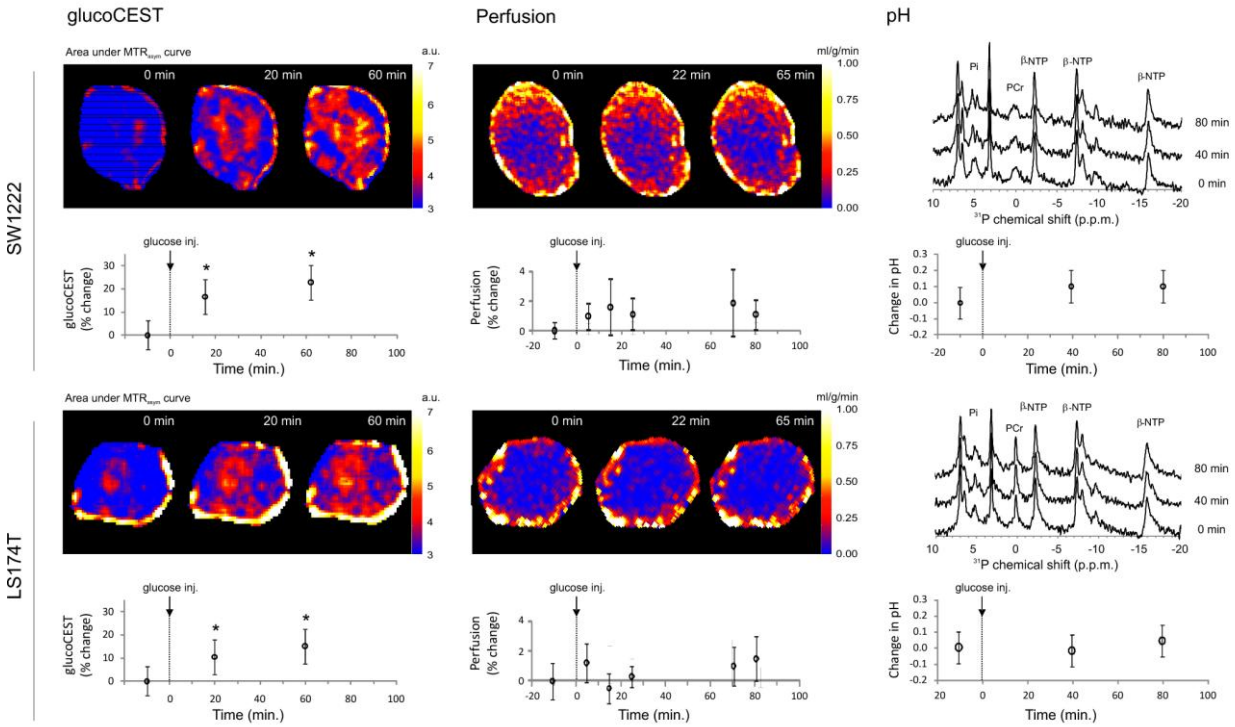

Supplemental Figure 6. The change in the area under the MTR_{asym} curve, intracellular pH and vascular perfusion with time, following injection of glucose. pH was measured using ^{31}P magnetic resonance spectroscopy, and example spectra, pre- and post-glucose injection (40 minutes and 90 minutes); vascular perfusion was measured using arterial spin labelling magnetic resonance imaging. Across the group of animals, median intracellular pH was 7.4 ± 0.8 for SW1222 and 7.0 ± 0.9 for LS174T tumors, which is consistent with the neutral or slightly basic intracellular pH generally reported in tumors [2-3]. No significant change in pH was measured following glucose uptake ($P > 0.05$, Mann-Whitney). Mean baseline tumor perfusion measured by ASL MRI was 0.42 ± 0.04 and 0.27 ± 0.02 mL g^{-1} min^{-1} in SW1222 and LS174T tumors, respectively, which were significantly different ($P < 0.05$, Mann-Whitney U-test). No significant change in perfusion was measured following glucose administration ($P > 0.05$, Mann-Whitney). These results show that, for the dose of glucose utilised in this study, concomitant effects due to hyperglycaemia (such as an increase in pH or blood flow) were negligible. All CEST data in this figure were acquired using the GE-CEST sequence.

Nature Medicine: doi:10.1038/nm.3252

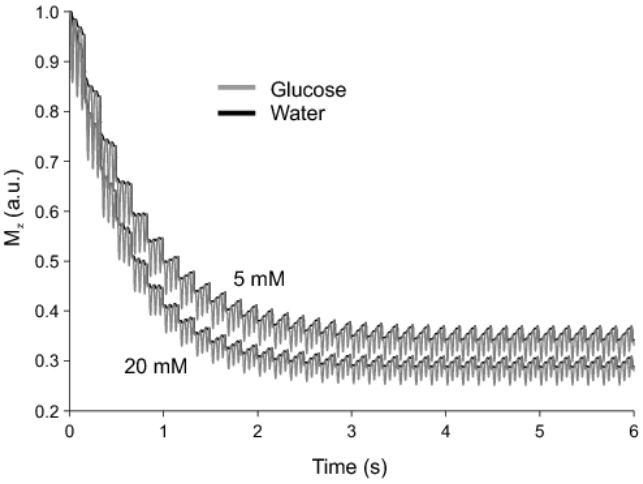

Supplemental Figure 7. Simulations of the longitudinal magnetisation of glucose and water pools during a gradient echo CEST (GE-CEST) acquisition, for both 5 and 20 mM glucose solutions. In a CEST experiment, labeling off-resonance from water requires irradiation of exchangeable proton resonances for a minimum period of a couple of seconds in order to allow the magnetization of the two proton pools to enter a steady state via bi-directional exchange [4-5]. The GE-CEST sequence used in this study is composed of a train of three, 50 ms Gaussian pulses, separated by a 2 ms delay, and followed by the gradient echo acquisition of a single line of k-space, with a total repetition time of 162.8 ms. Phase encoding was ordered linearly, so that the outer edge of k-space was acquired whilst the system entered a steady state. In order to ensure that a steady state condition was entered within minimal k-space acquisitions, the acquisition sequence was simulated using a two-pool model of proton exchange [6]. These simulations show that, for glucose concentrations of 5 and 20 mM, a steady state condition (defined as the longitudinal magnetization at the start of each repetition varying by less than 1%), is reached within 3 seconds, which corresponds to 19 k-space acquisitions. For the 128 phase encoding steps used in the GE-CEST sequence, this suggests that only the outer 13% of k-space is acquired prior to the steady condition being met.

Nature Medicine: doi:10.1038/nm.3252

SUPPLEMENTAL METHODS

GlucoCEST imaging parameters

For localization, tumors were imaged using a T_2-weighted fast spin echo sequence (repetition time 1.5 s; echo train length, 4; effective echo time, 17.2 ms; slice thickness, 1 mm; number of slices, 20; number of averages, 4; matrix size, 256 × 256; field of view, 30 × 30 mm^2).

For imaging with the GE-CEST sequence, a train of three Gaussian saturation pulses were applied, followed by the acquisition of a single line of k-space (repetition time, 162 ms; echo time 2 ms; saturation power, 1.5 μT; flip angle, 5°; field of view, 30 × 30 mm^2; slice thickness, 1 mm; matrix size, 128 × 128; saturation pulse bandwidth, 20 Hz). Lines from each image were acquired in a linear order. Data were acquired with 101 offset frequencies, ranging from -6 to +6 p.p.m. with respect to water, and separated by 0.12 p.p.m. Reference measurements were also acquired at a saturation offset of 200 p.p.m. (80,000 Hz), for normalizing signal intensity (4 averages). Alternatively, whole-tumour data from a single voxel were acquired with the EXPRESS sequence, using a train of 50 saturation pulses prior to readout, at the same saturation frequencies as used in the GE-CEST sequence. Other EXPRESS sequence parameters included: repetition time, 8 s; echo time 21.2 ms; saturation power, 1.5 μT; saturation time, 6 s; saturation pulse bandwidth, 20 Hz; readout bandwidth, 4 kHz.

The measured signal intensities were converted to the asymmetric magnetization transfer ratio (MTR_{asym}), given by

$$MTR_{asym}(t,\upsilon) = \frac{S^{+}(t,\upsilon) - S^{-}(t,\upsilon)}{S_{ref}(t,\upsilon_{ref})} \qquad [1]$$

where S^{+}, S^{-} and S_{ref} are signal intensities measured with saturation radiofrequency pulses centered at offset frequencies (ν) greater than 0 p.p.m. from water, less than 0 p.p.m. from water, or at the reference frequency, respectively, all of which are also functions of time, t. B_0 inhomogeneity correction was performed during post-processing by fitting cubic b-splines, identifying the location of the minimum water signal, and offsetting this point to 0 p.p.m. via cubic spline interpolation [7].

Dynamic data, where appropriate, were fitted to the following pharmacokinetic model [8], which is parameterized by S_0, r_1 and r_2:

$$GCE(t) = S_0(1 - e^{-r_1 t})e^{-r_2 t} \qquad [2]$$

Arterial spin labeling MRI

Arterial spin labeling (ASL) data were acquired using a FAIR Look-Locker ASL sequence with a single-slice spoiled gradient echo readout [9]. Sequence parameters included: echo time, 1.18 ms; inversion time spacing, 110 ms, first inversion time, 2.3 ms; 50 inversion recovery readouts. Geometrical parameters were matched to the GE-CEST sequence. A localized inversion thickness of 6 mm was used, followed by a global inversion slice thickness of 200 mm. The readout slice thickness was 1 mm. Perfusion maps were calculated using the quantitative model described by Belle *et al.* [10], assuming a blood-partition constant of 0.9. The longitudinal relaxation time (T_1) of capillary blood was assumed to be 1900 ms from previous measurements in the ventricular blood pool of the mouse heart [11]. Mean perfusion was calculated from tumor regions of interest, and perfusion maps were scaled between 0 and 1 mL g^{-1} min^{-1} for display.

^{31}P magnetic resonance spectroscopy

^{31}P magnetic resonance spectra were acquired using a dual-tuned ^{1}H/^{31}P surface coil positioned directly above the tumor. A pulse-acquire sequence was used, with the following parameters: excitation pulse width, 10 μs; power, 43.5 dB; acquisition bandwidth, 15 kHz; number of points, 3000; number of averages, 5000. Data were processed by application of a decaying exponential filter and reconstructed using Fourier transform. Peaks were fitted to a Lorentzian lineshape using JMRUI software [12-13] (phosphomonoester, inorganic phosphate, phosphodiester, phosphocreatine, γNTP, αNTP and βNTP), and intracellular pH quantified from the chemical shift between phosphocreatine and inorganic phosphate peaks, using the modified Henderson-Hasselbach relationship [14].

Dynamic contrast-enhanced MRI

Following an identical imaging setup and protocol as used in glucoCEST experiments, mice were administered a 50 mM solution of Gd-DTPA (Magnevist, Schering, Berlin) in saline as a bolus, via an intraperitoneal line (dose, 0.2 mmol kg^{-1}). Prior to injection, the baseline longitudinal relaxation rate R_1 was estimated by fitting a three parameter model to multiple inversion recovery Look-Locker data (echo time, 1.18 ms; inversion time spacing, 110 ms, first inversion time, 2.3 ms; 50 inversion recovery readouts). A spoiled gradient echo dynamic measurement was then performed, which included the following parameters: echo time, 1.8 ms; repetition time, 3.6 ms, flip angle, 20°; field of view, 30 × 30 mm^2; slice thickness, 1 mm; matrix size, 128 × 128.

Nature Medicine: doi:10.1038/nm.3252

The sequence was repeated for 5 minutes to measure baseline signal intensity, and then for another 60 minutes following injection of contrast agent. The mean baseline signal was used to relate signal intensity to the measured baseline R_1 and used to estimate the change in R_1 following delivery of Gd-DTPA. This was then converted to Gd-DTPA concentration using a relaxivity value of 2.9 s^{-1} mM^{-1} (from a previous *in vitro* measurement), and maps of the area under the enhancement curve (AUC) were produced.

Blood glucose measurements

Anaesthetized mice (isoflurane, 1.25% in O_2) were administered glucose via i.v. (n = 5) or i.p. (n = 5) injection, as per the method described for magnetic resonance imaging experiments. Approximately 0.1 μL of venous blood was sampled from a tail vein every 30 seconds for fifteen minutes prior to and 60 to 90 minutes following glucose administration. The concentration of glucose in blood samples was measured using a hand-held blood glucose analyzer (Roche, Welwyn, UK). Measurements prior to glucose injection were used to assess the stability of baseline blood glucose concentration. The change in blood glucose concentration from mean baseline signal was calculated for each animal and aggregated to provide a population average glucose concentration curve for each route of administration.

[^{18}F]-flurodeoxyglucose (FDG) autoradiography

Between 10 and 15 MBq of [^{18}F]FDG was administered i.p. in 0.3 mL of saline. [^{18}F]FDG was allowed to circulate for 60 minutes to mirror glucoCEST experiments, at which point tumors were rapidly excised. Throughout the procedure the orientation of the tumor was maintained relative to previous axial MRI measurements, and, following excision, tumors were snap-frozen using liquid nitrogen-cooled isopentane and cut in half along the longest axial diameter, corresponding to the MRI imaging slice. Four 20 μm sections from each half of the tumor were cut using a cryotome (Leica CM3050S) and positioned on a phosphor imaging plate (Molecular Dynamics). Standard curves for quantification of [^{18}F]FDG activity were produced by spotting serial dilutions of the administered dose (1, 0.1, 0.01 and 0.001 %), which was performed twice per imaging plate. Three tumors per imaging plate were processed simultaneously.

Phosphor plates were left for 12 hours and then scanned on a phosphorimager (Typhoon Trio+, GE Healthcare). Images were transferred to a desktop computer and analyzed using software developed in-house in the Interactive Data Language (IDL, Boulder, CO). The mean intensity, s, from each standard was measured and data were fitted with a function of the form $c = a \exp(b.s)$, where c is the concentration of [^{18}F]FDG and a and b are fitted parameters.

[U-^{13}C]glucose nuclear magnetic resonance spectroscopy of tumor fragments

[U-^{13}C]glucose (Sigma-Aldrich, Gillingham, UK) was administered i.p. to mice, following the *in vivo* glucoCEST protocol on the benchtop. At 60 minutes following injection, tumors were freeze-clamped, resected and stored at -80 °C. Following weighing, tumors were powdered in a percussion morter over liquid nitrogen and chloroform, methanol and water were added (1 mL per gram of tissue). Samples were transferred to a solvent-proof container and centrifuged for 5 minutes to allow the samples to separate into aqueous and organic phases. The upper and lower phases were withdrawn using a glass pipette and transferred to separate containers. Solvents were blown off with dry nitrogen gas and placed in a freeze drier for 8 hours to remove water and any remaining solvents. Samples were then freeze-dried, and D-chloroform and deuterium oxide added to aqueous and organic samples, respectively, and each were transferred to NMR tubes.

^{1}H-decoupled ^{13}C NMR spectra of the aqueous samples were acquired using a 500 MHz Bruker DRX spectrometer (Bruker, Karlsruhe, Germany). Acquisition parameters included: flip angle, 45°; sweep width, 26,300 Hz (209 p.p.m.); acquisition time 620 ms; relaxation delay, 2000 ms; number of averages, between 6000 and 20000. ^{13}C free induction decays were processed with a 3 Hz line broadening prior to Fourier transform. Spectra from each tumour type were combined and averaged and in-house software written in the Interactive Data Language (IDL, Boulder, California), to fit multiple Lorentzian lineshapes.

Immunofluorescence and Histochemical Analysis

Pimonidazole, a biomarker for hypoxia binding at approximately pO_2 < 10 mmHg, was administered i.p. (60 mg kg^{-1}) and allowed to circulate for 30 minutes prior to sacrifice in order to measure tumor hypoxia with fluorescence microscopy. The *in vivo* DNA-binding dye Hoechst 33342, used to demonstrate perfusion, was administered i.v. (10 mg kg^{-1}, Invitrogen) and allowed to circulate for 3 minutes before tumors were rapidly resected, cut in half, and one half snap-frozen in isopentane cooled with liquid nitrogen; the other half was fixed in formaldehyde.

Frozen tumor tissue was sectioned at 10 μm and stored at -80 °C. Tumor orientation relative to MRI scans

Nature Medicine: doi:10.1038/nm.3252

was maintained throughout sectioning and processing of tumors. After thawing, sections were fixed in acetone for 10 minutes and left to air dry at room temperature. After rinsing in phosphate-buffered serum (PBS), sections were incubated simultaneously with a 1:200 dilution Alexafluor 546 goat anti-rat antibody (Molecular Probes) and with a 1:2000 dilution of a FITC conjugated rabbit polyclonal anti-pimonidazole antibody. After rinsing in PBS, sections were mounted in PBS and viewed using an Axioimager microscope (Carl Zeiss, UK) at x10 magnification. Perfusion was viewed by a UV filter (365 nm excitation), and hypoxia by a FITC filter (450 – 490 nm excitation).

The percentage tumor hypoxia and perfusion were quantified by defining autofluoresence thresholds on pimonidazole and Hoechst 33342 images and counting the number of pixels with signal intensity greater than this threshold, per unit area of tumor tissue [15-16].

Image registration

GlucoCEST, [^{18}F]FDG autoradiography and fluorescence microscopy images were co-registered by resampling images to the resolution of the MRI data and manually overlaid using software written in-house in IDL. Tumor orientation was maintained throughout sectioning and tissue processing, and small deviations in alignment were corrected using an automated registration algorithm based on rigid body registration, with a mutual information cost function [17]. Images were co-registered by translation and rotation, with the latter constrained to $\pm 30°$ from its original orientation.

Glucose phantoms

Ten serial dilutions of glucose were prepared in distilled water, at concentrations ranging from 1 to 500 mM. Each of these solutions was prepared four times, each with a different pH of 6.4, 6.8, 7.2 or 7.6. pH was varied by the addition of dilute hydrochloric acid or potassium hydroxide and measured using a pH monitor (HI 2210, Hanna Instruments Ltd., Bedfordshire, UK). For MRI scanning, four glucose concentrations were measured per imaging session and were sealed in 5 mL pyrex containers. These were positioned in a 50 mL Falcon tube filled with distilled water.

During MRI scanning, the temperature of the scanner bore and of the phantoms was maintained at 37°, which was monitored by inserting a temperature probe inserted into the Falcon tube. Approximately 30 minutes was required for phantoms to equilibrate from room temperature, after which shimming of the magnetic field was performed and images were acquired using the same GE-CEST sequence as used *in vivo*. The glucoCEST enhancement (GCE) is defined as the change in the integral of MTR_{asym} between 4 and 0.75 p.p.m with time, following glucose administration at $t = 0$:

$$GCE(t) = \int_{0.75}^{4} MTR_{asym}(t,\upsilon)d\upsilon - \int_{0.75}^{4} MTR_{asym}(0,\upsilon)d\upsilon \quad [3]$$

MTR_{asym} image data were converted to GCE maps and regions of interest were drawn corresponding to each separate glucose phantom. The mean GCE was calculated for each and plotted as a function of glucose concentration, and were fitted using linear regression for each pH value measured.

Imaging phantoms were also constructed containing solutions of glucose, glucose 6-phosphate, fructose 6-phosphate and fructose 6,1-biphosphate (Sigma-Aldrich, Gillingham, UK), which were prepared at a range of concentrations (20 to 200mM) and pH = 7.4, and were scanned at 37 °C.

A similar procedure was also followed for solutions of glucose in blood serum. Here, 25 mL of blood was withdrawn from two female rats by cardiac puncture and separated using a centrifuge. Plasma was withdrawn and its glucose concentration measured using a hand-held blood glucose analyzer (Roche, Welwyn, UK). The pH of the samples was set to 7.4 as described above, and samples maintained at 37 °C during scanning.

Simulation of the glucoCEST imaging sequence

The evolution of the longitudinal magnetisation of glucose and water were simulated using software written in-house in Matlab (Mathworks, Massachusetts, USS). A modified form of the Bloch equations incorporating glucose and water proton pools [6] exchanging at a rate k_1 = 1000 Hz, were numerically solved for two concentrations of glucose. Labelling and readout pulses were simulated according to those used in the GE-CEST sequence (see main Methods section), with labelling pulses centered at 1.2 p.p.m. from water. Other parameters in the model included the T_1 and T_2 of water (2000 and 30 ms, respectively) and the T_1 and T_2 of glucose (400 and 6 ms, respectively [18]).

SUPPLEMENTAL REFERENCES

1. Ali, M.M., Liu, G., Shah, T., Flask, C.A. & Pagel, M.D. Using two chemical exchange saturation transfer magnetic resonance imaging contrast agents for molecular imaging studies. *Accounts of chemical research* **42**, 915-924 (2009).

2. Gillies, R.J., Liu, Z. & Bhujwalla, Z. 31P-MRS measurements of extracellular pH of tumors using 3-aminopropylphosphonate. *Am J Physiol* **267**, C195-203 (1994).
3. Gillies, R.J., Raghunand, N., Garcia-Martin, M.L. & Gatenby, R.A. pH imaging. A review of pH measurement methods and applications in cancers. *IEEE Eng Med Biol Mag* **23**, 57-64 (2004).
4. Zhou, J., Wilson, D.A., Sun, P.Z., Klaus, J.A. & Van Zijl, P.C. Quantitative description of proton exchange processes between water and endogenous and exogenous agents for WEX, CEST, and APT experiments. *Magn Reson Med* **51**, 945-952 (2004).
5. Sun, P.Z., Farrar, C.T. & Sorensen, A.G. Correction for artifacts induced by B(0) and B(1) field inhomogeneities in pH-sensitive chemical exchange saturation transfer (CEST) imaging. *Magn Reson Med* **58**, 1207-1215 (2007).
6. Henkelman, R.M.*, et al.* Quantitative interpretation of magnetization transfer. *Magn Reson Med* **29**, 759-766 (1993).
7. Stancanello, J.*, et al.* Development and validation of a smoothing-splines-based correction method for improving the analysis of CEST-MR images. *Contrast media & molecular imaging* **3**, 136-149 (2008).
8. Kurland, R., Shoop, JD, Funkhouser, GR. A kinetic model for time development of Gd-DTPA relaxation enhancement. *Proceedings of the Seventh Annual Meeting of the SMRI*, 177 (1989).
9. Campbell-Washburn, A.E.*, et al.* Cardiac arterial spin labeling using segmented ECG-gated Look-Locker FAIR: Variability and repeatability in preclinical studies. *Magn Reson Med* (2012).
10. Belle, V.*, et al.* In vivo quantitative mapping of cardiac perfusion in rats using a noninvasive MR spin-labeling method. *J Magn Reson Imaging* **8**, 1240-1245 (1998).
11. Campbell, A.E.*, et al.* Equilibrium contrast CMR for the detection of amyloidosis in mice. *Journal of Cardiovascular Magnetic Resonance* **13**, O60 (2011).
12. Naressi, A.*, et al.* Java-based graphical user interface for the MRUI quantitation package. *MAGMA* **12**, 141-152 (2001).
13. Naressi, A., Couturier, C., Castang, I., de Beer, R. & Graveron-Demilly, D. Java-based graphical user interface for MRUI, a software package for quantitation of in vivo/medical magnetic resonance spectroscopy signals. *Comput Biol Med* **31**, 269-286 (2001).
14. De Graaf, A.M.A. *In vivo NMR spectroscopy: principles and techniques*, (John Wiley & Sons Ltd., Chichester, 2008).
15. Walker-Samuel, S.*, et al.* Non-invasive in vivo imaging of vessel calibre in orthotopic prostate tumour xenografts. *International journal of cancer* **130**, 1284-1293 (2012).
16. Burrell, J.S.*, et al.* Investigating temporal fluctuations in tumor vasculature with combined carbogen and ultrasmall superparamagnetic iron oxide particle (CUSPIO) imaging. *Magn Reson Med* **66**, 227-234 (2011).
17. Pluim, J.P., Maintz, J.B. & Viergever, M.A. Mutual-information-based registration of medical images: a survey. *IEEE transactions on medical imaging* **22**, 986-1004 (2003).
18. McMahon, M.T.*, et al.* Quantifying exchange rates in chemical exchange saturation transfer agents using the saturation time and saturation power dependencies of the magnetization transfer effect on the magnetic resonance imaging signal (QUEST and QUESP): Ph calibration for poly-L-lysine and a starburst dendrimer. *Magn Reson Med* **55**, 836-847 (2006).

Nature Medicine: doi:10.1038/nm.3252